Pamukkale Univ Muh Bilim Derg, 30(2), 174-181, 2024

Pamukkale Üniversitesi Mühendislik Bilimleri Dergisi

Pamukkale University Journal of Engineering Sciences

Color images denoising using complementary color wavelet transform

Tamamlayıcı renk dalgacık dönüşümü kullanılarak renkli görüntülerin gürültüden arındırılması

Mücahit CİHAN[1*], *Murat CEYLAN*[1]

[1]Department of Electrical-Electronics Engineering, Faculty of Engineering and Natural Sciences, Konya Techn. Univ., Konya, Turkey.
mcihan@ktun.edu.tr, mceylan@ktun.edu.tr

Received/Geliş Tarihi: 14.09.2022 Revision/Düzeltme Tarihi: 24.03.2023 doi: 10.5505/pajes.2023.27460
Accepted/Kabul Tarihi: 26.05.2023 Research Article/Araştırma Makalesi

Abstract

The RGB color ring is known as the most understandable color representation in human vision, as it has complementary colors. However, color relationships hardly ever play a function in wavelet-primarily based totally color image processing tools. In this study, Complementary Color Wavelet Transform (CCWT), which is supported by complementary color relationships and complex wavelet design techniques, is used to denoise in color images. This wavelet consists of a family of two-dimensional complex wavelets with a phase difference of 2π/3 obtained from the angle relationship between the color axes of the RGB color ring, and is very effective in terms of directional selectivity. By using the coefficients of the directions in different phases, denoising processes are performed from the multi-channel color images. It was validated the performance of CCWT using various color images and noise levels, based on peak signal-to-noise ratio, structural similarity index, mean square error values, and visual quality. CCWT was compared with state-of-the-art multi-resolution image denoising algorithms, and found that the method achieves superior denoising performance both quantitatively and visually. It was also analyzed the computation time of CCWT and compared it with existing approaches.

Keywords: Complementary color wavelet transform, Color image denoising, Wavelet thresholding, Gaussian noise.

Öz

RGB renk halkası, tamamlayıcı renklere sahip olduğu için insan görmesinde en anlaşılabilir renk temsili olarak bilinmektedir. Bununla birlikte, renk ilişkileri, dalgacık tabanlı renkli görüntü işleme araçlarında neredeyse hiç rol oynamamaktadır. Bu çalışmada tamamlayıcı renk ilişkileri ve kompleks dalgacık tasarım tekniklerine dayanan, Tamamlayıcı Renk Dalgacık Dönüşümü (TRDD), renkli görüntülerde gürültülerin giderilmesi için kullanılmıştır. Bu dalgacık, RGB renk halkasında bulunan renk eksenleri arasındaki açı ilişkilerinden elde edilen 2π/3 faz farklarına sahip, 2 boyutlu kompleks dalgacıklardan oluşan bir aileden meydana gelmektedir ve yönsel seçicilik bakımdan çok etkilidir. Farklı fazdaki yönlere ait katsayılar kullanılarak çok kanallı renkli görüntülerden gürültü giderme işlemleri gerçekleştirilmiştir. Farklı renkli görüntüler ve gürültü seviyeleri kullanılarak TRDD'nin performansı, tepe sinyal-gürültü oranı, yapısal benzerlik indeksi, ortalama kare hata değerleri ve görsel kaliteye dayalı olarak doğrulanmıştır. TRDD, en gelişmiş çok çözünürlüklü görüntü gürültü giderme algoritmalarıyla karşılaştırılmış ve yöntemin hem niceliksel hem de görsel olarak daha üstün gürültü giderme performansı elde ettiği görülmüştür. Ayrıca TRDD'nin hesaplama süresi analiz edilmiş ve mevcut yaklaşımlarla karşılaştırılmıştır.

Anahtar kelimeler: Tamamlayıcı renk dalgacık dönüşümü, Renkli görüntü gürültü giderme, Dalgacık eşikleme, Gauss gürültüsü.

1 Introduction

The images obtained using sensors may be distorted by noise sources. There is a significant reduction in the quality of images distorted by noise. It is aimed to increase the image quality by denoising with different image processing techniques. Traditionally, linear filters (such as mean, median, etc.) are used to denoise from images, but this blur the data [1]. Some methods such as domain transform [2], non-local algorithm [3] are used for image denoising applications. These methods have the disadvantages of manually setting parameters and resorting to complex optimization.

In image denoising research, it is a conventional practice to introduce artificial noise to a pristine image, which serves as a test image for evaluation purposes. This method grants researchers the ability to regulate the type and level of noise and facilitates the comparison of various denoising methods on the same test image. Although this approach does not precisely replicate the noise characteristics of the sensor, it is still a viable technique for assessing the effectiveness of different denoising methods.

With the advancement of image acquisition technology, color images are increasingly popular, leading to a growing demand for color image processing [4],[5]. In the fields of computer vision and image processing, image denoising is an important and fundamental research topic with certain theoretical value and practical importance [6]. Denoising technology not only improves the visual quality of the images but also provides more accurate and reliable data for image processing. For this reason, different wavelet-based methods have been used to denoise in color images in many studies in the literature and it is aimed to obtain successful results [7]-[9].

Wavelet transform is a signal processing technique that can represent signals in both the time and frequency domains [10]. Wavelet transform shows superior performance compared to other time-frequency analysis methods. This is because, especially in image processing applications, the time scale width of the window used can be adjusted to match the original signal [11]. This makes the wavelet transform useful for analysis of non-stationary signals.

Today, many image processing methods through grayscale channels have been suggested and examined in the literature.

*Corresponding author/Yazışılan Yazar

Different wavelet transform methods have been used to denoise in color images: Wavelet Packet-Based Noise Reduction Algorithm [12], Multiresolution Monogenic Wavelet Transform [7], Densely Self-Guided Wavelet Network [13]. When a color image needs to be processed, in a three-channel system for example RGB, LAB and YCbCr, each channel is considered a gray scale channel [14]. Grayscale image processing-based techniques are then applied to each color channel separately, without any changes. The overall result is obtained by summing or summing the squares of the three separate responses with little regard for the relationship between channels. Lack of color associations, edge displacements and color distortions etc. have many undesirable side effects [15].

In this study, a new wavelet transform method named Complementary Color Wavelet Transform (CCWT) proposed by Chen et al. [12] is used. CCWT employs a family of 2D complex wavelets with phase differences of 2π/3, based on the angle relationship between the color axes of the RGB color ring [12]. CCWT has better and more useful directional selectivity. It can also achieve better shift-invariant properties than the double-tree complex wavelet transform and the conventional discrete wavelet transform. Therefore, multi-resolution capabilities, the coefficient between directional color filtering, and color channels can be obtained by statistical modeling. By applying thresholding to the directional coefficients obtained because of CCWT, denoising from the images can be achieved.

The main contributions of this article can be described as follows.

- CCWT, a novel tool for color image analysis and processing, which is utilized for the first time in this study for color image denoising,
- The efficiency and visual quality of the results obtained using CCWT are compared with those obtained from other state-of-the-art methods in the literature. The comparison proves that the used method achieves superior results,
- The rich and practical direction selectivity of the CCWT coefficients enables the used method to effectively denoise images. Therefore, CCWT can be employed efficiently in denoising applications,
- While the computation time of the CCWT is viewed as a limitation, it may be more appropriate for applications such as medical or scientific research where its duration is not as critical.

2 Complementary colors

Intermediate colors opposite the primary colors in the color ring are called complementary colors and are one of the oldest color relationships defined [16]. Introduced by the International Commission on Illumination (CIE) in 1931, the R, G, B three-color system and color ring is one of the most commonly preferred color systems. White color can be obtained by mixing any 2 colors on the RGB color ring that the difference as much as the π angle [12]. This indicates that for complementary color applications, the RGB color system is well suited. Some studies show that complementary color relationships have a very important place in terms of color mixing, perception, and constancy [17],[18].

Figure 1 depicts the color ring of the RGB three-color system. As shown in Figure 1(a), the R, G, and B axes are oriented along the ring at 0, 2π/3, and 4π/3 angles, respectively. The color ring represents relationships between half-intensity and fully saturated colors. If another intensities and saturations need to be considered, the color ring representation can be enlarged to the very commonly preferred HSV (hue-saturation-value) color model representation. The HSV model can be represented by a conical or spherical model. The cone pattern is shown in Figure 1(b). The hue is in the circle at the top of the cone, the value is represented by the length of the cone, and the saturation is measured by the distance from the beginning point of the color. In the color ring or HSV color cone, any two colors with a difference of a π angle form a complementary pair. Of the complementary pairs, the four most important are Blue-Yellow, Green-Magenta, Red-Cyan, and Black-White, as they play a crucial role in color perception and human vision.

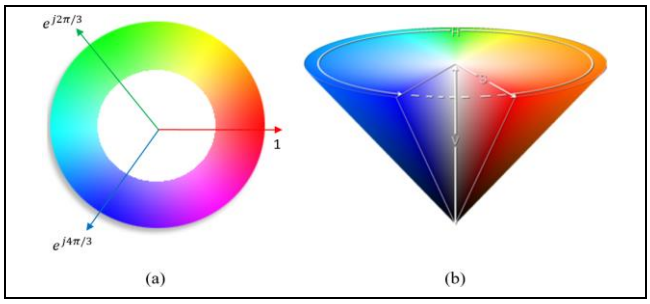

Figure 1. Complementary color representation. (a): Cartesian coordinate system RGB color ring and R, G, B axes. (b): HSV color cone model.

3 Structure and properties of CCWT

CCWT is a 2D wavelet transform-based method. In the classical 2D Discrete Wavelet Transform (DWT), the lowpass operator *L(.)* and the highpass operator *H(.)* are applied across two dimensions to decompose a 2D grayscale image into three wavelet subbands, LH, HL, HH, and a scale subband, LL.

The LL subband obtained from the 2D DWT is further decomposed into four subbands: LLH, LHL, LHH, and LLL. The evaluation technique of a discrete wavelet transform level is proven in Figure 2. The HL and LH subbands of the discrete wavelet transform are oriented horizontally and vertically and can detect horizontal and vertical changes in an image. However, the HH subband is incapable of isolating the ±45 direction. Therefore, it is weak in terms of directional selectivity.

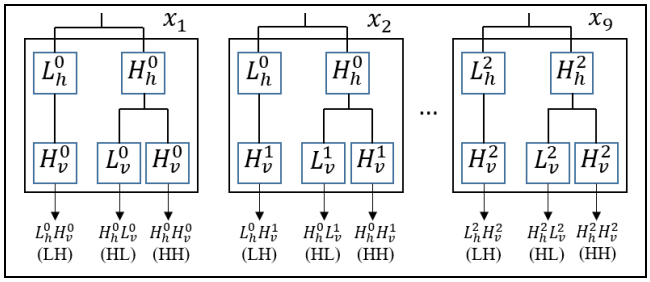

Figure 2. Nine 2D discrete wavelet transform decomposition examples with different phase combinations.

In Figure 2, 2D discrete wavelet transform is applied to different phase differences (0, 2π/3 and 4π/3). Each DWT decomposition block represents 3 discrete wavelet transform subbands x_n, *n = 1, 2, ..., 9*. Corresponds to 0 = 0, 1 = 2π/3, and 2 = 4π/3 on low and high pass functions. Then, because of obtaining the HH, HL and LH subbands, the collection of 9

discrete wavelet transform decompositions in various combinations and the process of finding 16 single-channel (LH, HL, HH respectively 6, 6, 4) two-dimensional CCWT subbands is performed (Figure 3). These subbands contain coefficients of different orientations.

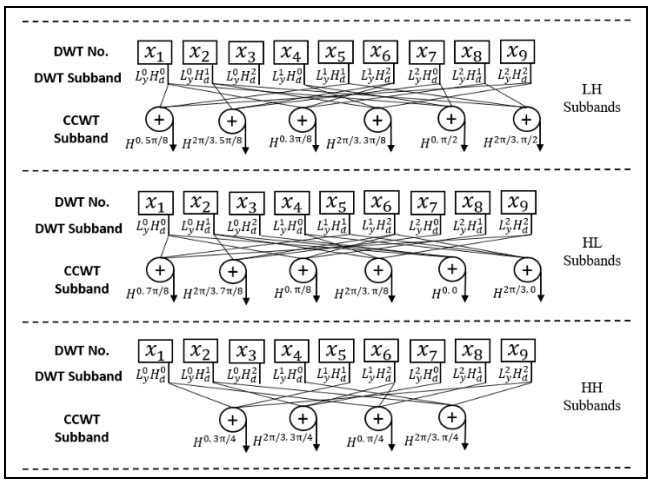

Figure 3. The flowchart for the two-dimensional CCWT analysis at each level, showing the sixteen two-dimensional single-channel CCWT subbands obtained from nine DWT decompositions.

After obtaining the two-dimensional CCWT coefficients, wavelet thresholding is applied to these coefficients. Then, a denoised image is obtained by inverse CCWT and inverse DWT operations. The flowchart for image denoising is shown in Figure 4.

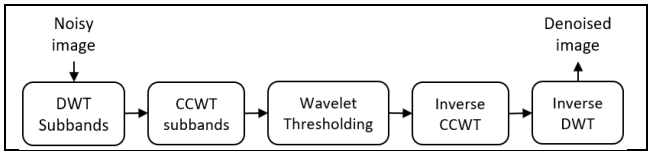

Figure 4. The flowchart for image denoising.

4 Application results and discussion

In this section, all applications are run on six color test images of 512 × 512: “Lena”, “Peppers”, “Baboon”, “Parrots”, “Twins” and “Airplane”. The images in question are presented in Figure 5.

Figure 5. Color test images called “Lena”, “Peppers”, “Baboon”, “Parrots”, “Twins” and “Airplane” used in the applications (the images are ordered left to right, top to bottom according to their names).

Then zero-mean white Gaussian noise is added at the $\sigma \in \{20, 25, 30, 35, 40\}$ levels. To assess the denoising performance, three metrics were used: Peak Signal-to-Noise Ratio (PSNR), Structural Similarity Index (SSIM), and Mean Square Edüzenlendirror (MSE).

Peak Signal-to-Noise Ratio (PSNR): PSNR is an objective performance evaluation criteria that provides a score of loss information in decibels (dB). A higher PSNR value indicates less distortion [19]. If x represents the original image, y represents the resulting image, σ represents the standard deviation, and E represents the error, then PSNR is calculated as follows:

$$PSNR(x,y) = 20\log\left(\frac{255}{\sigma\left(\sum_i^M \sum_{j=1}^N (E_{x(i,j)} - E_{y(i,j)}\right)}\right) \quad (1)$$

Structural Similarity Index (SSIM): SSIM is calculated by analyzing various windows of an image. For two windows x and y with common dimensions NxN, let μ_x be the mean of x, let σ_x^2 and σ_{xy} be the variance of x and the covariance of x and y. SSIM between x and y signals:

$$SSIM\ (x,y) = \frac{(2\mu_x\mu_y + c_1)(2\sigma_{xy} + c_2)}{(\mu_x^2\mu_y^2 c_1)(\sigma_x^2\sigma_y^2 c_2)} \quad (2)$$

Mean Squared Error (MSE): MSE measures the amount of error between two images. MSE evaluates the mean square difference between observed and predicted values. A lower MSE means a better image. While R and C represent the number of rows and columns of x and y images, MSE is expressed as the following:

$$MSE(x,y) = \frac{1}{RC}\sum_{i=1}^{R}\sum_{j=1}^{C}(x_{i,j} - y_{i,j})^2 \quad (3)$$

For this study, denoising was performed with CCWT using color test images. After adding gaussian noise to the color image, the R, G, and B channels in the image were split and the direction coefficients were obtained by applying CCWT to these channels. Level 5 decomposition process was applied to all images. Then, by applying wavelet thresholding to these coefficients, the channels are denoised and concatenated with inverse CCWT to obtain a denoised image.

To demonstrate the effectiveness and visual quality of the CCWT method; the Discrete Wavelet Transform (DWT), Monogenic Wavelet Transform (MWT) [20],[21], Curvelet Transform (CT) [22] and WaveAtom Transform (WAT) [23] are compared.

4.1 Discrete wavelet transform (DWT)

The DWT is used to transform a discrete-time signal from the time domain to the time-frequency domain. This transform allows for spectrum analysis and analysis of the spectral behavior of the signal over time. The DWT decomposes the signal into two components: low-pass components and high-pass components. Both of these components contain information about the original signal.

The low-pass components correspond to the smoothness in the image, while the high-pass components capture the sharp changes in the image, such as edges [24].

In a DWT in [25], the values of $j = 2^l$ and $k = 2^l p$ mean expansion and translation, respectively, where l and p are integers. two-dimensional squares $d(l,p)$ is called the DWT of $f_{(n)}$, which is shown in Equaiton 4. $\psi(n) \in L^2(R)$ is limited in

time domain mother wavelet function in the time domain and has values at a certain range, otherwise it is zero.

$$f_{(n)} = \sum_{l=-\infty}^{\infty} \sum_{p=-\infty}^{\infty} d_{(l,p)} 2^{\frac{-l}{2}} \quad (4)$$

4.2 Monogenic wavelet transform (MWT)

The monogenic signal is a two-dimensional extension of the analytical signal, with the added feature of rotational invariance. Given a two-dimensional true value signal $f(x,y)$, the corresponding monogenic signal $g(x,y)$ is defined as a three-component signal, as follows.

$$f_M(x,y) = \begin{bmatrix} f(x,y) \\ \Re\{R_{ez}(f)\} \\ \Re\{S_{ez}(f)\} \end{bmatrix} = \begin{bmatrix} A cos\phi \\ A sin\phi cos\theta \\ A sin\phi sin\theta \end{bmatrix} \quad (5)$$

Where $R_{ez}(f)$ and $S_{ez}(f)$ denote the real part and imaginer part of the Riesz transform of the complex value of the two-dimensional signal f, $A = \sqrt{f^2 + |R_{ez}(f)|^2}$ is the local amplitude, $\theta = \arg\{R_{ez}(f)\}$ is the local orientation, and $\phi = \arg\{f + i|R_{ez}(f)|\}$ is the local phase.

As stated in [26], the MWT is generated by integrating the gradient operator and the Riesz transform. For a given two-dimensional signal $f(x,y)$, the gradient of $f(x,y)$ is defined as follows:

$$\nabla f(x,y) = \left[\frac{\partial f(x,y)}{x} \quad \frac{\partial f(x,y)}{y}\right] \quad (6)$$

Then, the edge force M and the orientation angle θ can be used to determine the local maximum variation of $f(x,y)$, as follows:

$$\begin{cases} M = \sqrt{f_x(x,y)^2 + f_y(x,y)^2} \\ \theta = \arg\{f_x(x,y) + i * f_y(x,y)\} \end{cases} \quad (7)$$

Where f_x and f_y are partial derivatives of $f(x,y)$. To perform monogenic analysis, a bandpass filter is used to select a specific scale for analysis. The isotropic poly-harmonic spline wavelet is utilized as a smoothing kernel, as defined in [27]. As previously discussed, the wavelet domain extension is achieved using marginal Riesz features. The subband decompositions of the monogenic wavelet are presented below:

$$\begin{cases} \hat{H}(z) = H(z) \overset{F}{\leftrightarrow} \exp\left(-\frac{\omega^2 \sigma_i^2}{2}\right) \\ \hat{G}(z) = G(z) \overset{F}{\leftrightarrow} \sqrt{1 - H(z)^2} \end{cases} \quad (8)$$

The monogenic wavelet coefficients consist of three parts: the amplitude, as well as two phases. One of the phases is responsible for recording local displacement information, while the other phase is responsible for describing the geometric properties of the image structure. In contrast, the amplitude reflects the dependability of the two phases of any scalar signal at any given scale.

4.3 Curvelet transform (CT)

The CT is a multi-scale, multi-directional transform used for image and signal processing. It is designed to efficiently represent curved edges, which are difficult to represent using traditional transforms. The curvelet transform uses a combination of the wavelet transform and the ridgelet transform [28] to decompose an image or signal into increasingly fine scales and directions, allowing for a more complete representation of its features. The digital realization of the curvelet transform involves four stages:

Subband decomposition: To filter the f image into subbands using the à trous algorithm [29], a set consisting of a low pass filter P_0 and band pass filters Δ_s, where $s \geq 0$, is defined:

$$f \mapsto (P_0 f, \Delta_1 f, \Delta_2 f, \dots) \quad (9)$$

Smooth partitioning: Each subband is meticulously windowed into binary frames:

$$h_Q = W_Q . \Delta_s f, \quad \forall Q \in Q_s \quad (10)$$

Where W_Q is a collection of the smooth windowing function and Q denotes a binary function that is a collection of Q_s binary squares on the scale s:

$$Q_{(s,k_1,k_2)} = \left[\frac{k_1}{2^s}, \frac{k_1+1}{2^s}\right] * \left[\frac{k_2}{2^s}, \frac{k_2+1}{2^s}\right] \quad (11)$$

Renormalization: Each binary square is renormalized to $[0,1]^2$ unit scale using the function:

$$g_Q = T_Q^{-1} . h_Q \quad (12)$$

Where $(T_Q f)(x_1, x_2) = 2^s f(2^s x_1 - k_1, 2^s x_2 - k_2)$ is the renormalization operator.

Ridgelet analysis: The two-dimensional ridgelet transform in R^2 can be defined as:

For every $a > 0$, every $b \in R$, and every $\theta \in [0, 2\pi)$, the bivariate projection $\Psi_{a,b,\theta}: R^2 \to R^2$ can be defined as:

$$\Psi_{a,b,\theta}(x) = a^{\frac{1}{2}} \Psi\left(\frac{x_1 cos\theta + x_2 sin\theta - b}{a}\right) \quad (13)$$

Where a, b, and θ are the scale, position, and direction parameters, respectively, and Ψ is the wavelet function. These projections are constant along the $x_1 cos\theta + x_2 sin\theta = const$ lines and are wavelets in the orthogonal direction.

The ridgelet coefficients $f(x_1, x_2)$ for a given function can be defined as:

$$R_f(a,b,\theta) = \int f(x_1,x_2) \Psi_{(a,b,\theta)}(x_1,x_2) dx_1 dx_2 \quad (14)$$

A simple change in variables shows that the ridgelet coefficients of the function f are given by analysis of the Radon transform as:

$$R_f(a,b,\theta) = \int R_f(t,\theta) a^{1/2} \Psi(\tfrac{t-b}{a}) \mathrm{dt}) \quad (15)$$

Where t is the variable and R_f is the Radon transform defined as:

$$R_f(t,\theta) = \int f(x_1,x_2) \delta(x_1 cos\theta + x_2 sin\theta - t) dx_1 dx_2 \quad (16)$$

δ is the Dirac distribution.

The Ridgelet transform is a technique that involves applying a one-dimensional wavelet transform to the Radon transform slices when the orientation variable is fixed and depends on the variable t. The Radon transform [30] can be obtained by

implementing a one-dimensional inverse Fourier transform on a two-dimensional Fourier transform that is limited by radial lines passing through the origin.

In the field of CT, two denoising methods have been developed [31]. The first approach involves hard thresholding of the curvelet coefficients, while the second approach involves loop rotation applied to the noisy image before the CT is performed.

4.4 Wave atom transform (WAT)

The WAT is a type of wavelet transform that employs a set of atoms with distinct properties to represent images. In contrast to the conventional DWT, which utilizes fixed basis functions, the WAT employs adaptive basis functions that are better suited to capturing the unique features of an image. This enables the WAT to achieve superior performance in image compression, denoising, and feature extraction applications.

The WAT is differentiated from other transforms by employing two parameters (α, β) to define the wave packet families, which index numerous wavepacket architectures. The α parameter determines whether the parsing is multi-scale, while the β parameter determines whether the core elements of a transformation are localized and poorly directional or extended and fully directional. Figure 6 [32] illustrates the location of the wave atom and other transformations relative to α and β. If α is equal to 1, the decomposition is multi-scale, whereas if α is equal to 0, the parsing is not multi-scale. On the other hand, if β is equal to 1, the base element is localized and sharp, while if β is equal to 0, the principal element is extended and fully directional.

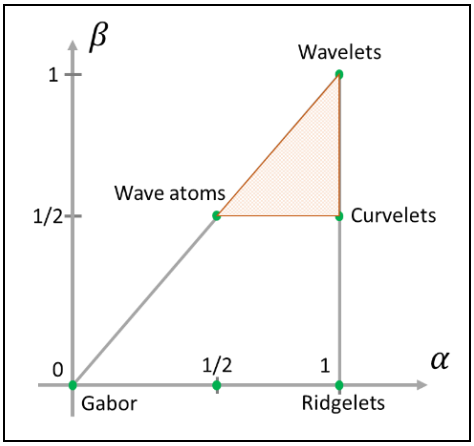

Figure 6. Representation of different transformations based on the index parameters (α, β).

Wave atoms are capable of capturing both the consistency of a pattern throughout oscillations and its pattern throughout said oscillations. To define a two-dimensional wave atom formally, it can be represented as $\phi_\mu(x)$ with the subscript $\mu = (j, m, n) = (j, m_1, m_2, n_1, n_2)$. All of the five quantities, namely j, m_1, m_2, n_1, n_2 are integer values that index a point (x_μ, ω_μ) in phase space;

$$x_\mu = 2^{-j}n, \quad \omega_\mu = \pi 2^j m, \quad C_1 2^j \le \max_{i=1,2}|m_i| \le C_2 2^j \tag{17}$$

Where C_1 and C_2 are two positive constants, x_μ is the position vector and the center of $\varphi_\mu(x)$, and the wave vector ω_μ determines the centers of both bumps of $\hat{\varphi}_\mu(x)$ as $\pm\omega_\mu$ [32]. Elements of the frame of wave packets $\{\varphi_\mu\}$ are called wave atoms when:

$$\begin{aligned}\left|\hat{\varphi}_\mu(\omega)\right| \le C_M.2^{-j}\left(1+2^{-j}\left|\omega+\omega_\mu\right|\right)^{-M} \\ + C_M.2^{-j}\left(1+2^{-j}\left|\omega-\omega_\mu\right|\right)^{-M}\end{aligned} \tag{18}$$

$$\left|\varphi_\mu(x)\right| \le C_M.2^{j}\left(1+2^{j}\left|x-x_\mu\right|\right)^{-M}, \text{for all } M>0 \tag{19}$$

$$\begin{aligned}\psi_m^0(\omega) = e^{-i\omega/2}\Bigg[e^{i\alpha_m}g\left(\varepsilon_m\left(\omega-\pi\left(m+\frac{1}{2}\right)\right)\right) \\ + e^{-i\alpha_m}g\left(\varepsilon_m \right. \\ \left. + 1\left(\omega+\pi\left(m+\frac{1}{2}\right)\right)\right)\Bigg]\end{aligned} \tag{20}$$

Where $\varepsilon_m = (-1)^m$ and $\alpha_m = \frac{\pi}{2}(m+\frac{1}{2})$ [32]. A convenient real-valued function, which has compact support on an interval of length 2π, is chosen as the g function in the following manner:

$$\sum_m |\psi_m^0(\omega)|^2 = 1 \tag{21}$$

For this study, three distinct experiments were performed. Within the 1st experiment, all color test images were distorted by adding Gaussian white noise. The results of denoising for the "Lena" and "Baboon" color test images are shown in Figures 7 and Figure 8, respectively.

Figure 7. Denoising results (σ = 30) for the color image “Lena” using different algorithms. Original image, noisy image, DWT, MWT, CT, WAT and CCWT. (Left to right, top to bottom).

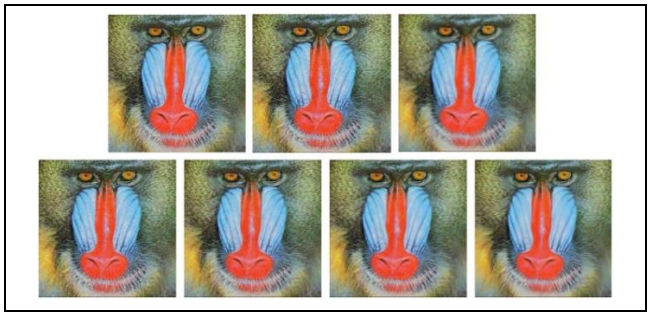

Figure 8. Denoising results (σ = 30) for the color image “Baboon” using different algorithms. Original image, noisy image, DWT, MWT, CT, WAT and CCWT. (Left to right, top to bottom).

In the meantime, the results of denoising for the "parrot" and "airplane" color test images are shown in Figures 9 and 10, respectively. Meanwhile, the denoised results of the “Parrot” and “Airplane” color test images are given in Figures 9 and 10, respectively.

Figure 9. Denoising results (σ = 30) for the color image "Parrots" using different algorithms. Original image, noisy image, DWT, MWT, CT, WAT and CCWT. (Left to right, top to bottom).

Figure 10. Denoising results (σ=30) for the color image "Airplane" using different algorithms. Original image, noisy image, DWT, MWT, CT, WAT and CCWT. (Left to right, top to bottom).

It can be seen that CCWT gives better results in homogeneous regions and produces smoother surfaces. In contrast, all denoising algorithms contain many artifacts under high noise levels, while CCWT and WAT contain comparatively few artifacts. CCWT can retain a lot of image details compared to DWT, MWT, CT, and WAT, particularly in Figures 9 and 10. When Figures 7, 8, 9 and 10 are examined, CCWT method gives better results in denoising in images compared to other methods.

Although the utilized denoising method resulted in high denoising performance, certain regions of the images, such as the lower right part of the "Baboon" and some portions of the "Parrot", exhibited blurring. The loss of image detail due to denoising is a known issue that can include edge smoothing and the loss of fine details. This occurs because most denoising methods rely on thresholding or averaging to reduce noise, which can inadvertently affect other areas of the image. Nevertheless, it is evident that the applied method yields a higher quality image that is free from noise.

The 2nd experiment compared CCWT with alternative denoising methods at different noise levels to prove its effectiveness. Table 1 shows PSNR, SSIM and MSE values for various color test images with different noise levels. As can be easily seen, the CCWT method performs better regardless of the noise level. It can be understood from this table that successful PSNR and SSIM values are obtained even with an increase in the σ value. However, it is seen that MSE values increase excessively at high σ values. Since the denoising algorithm used in this study contains subbands of different orientations, it gave more successful results in denoising in color images compared with other methods. Additionally, the fact that CCWT has the advantage of being able to better discriminate phase information in color images is also a key factor in this success.

The 3rd experiment evaluates the computation time of different color denoising methods. Approximate times were calculated using MATLAB on an NVIDIA GeForce GTX 1080 Ti running Windows 10 and a desktop workstation with 64 GB of RAM. Table 2 shows the time required to process different color test images with different algorithms. It is obvious that CCWT has less computation time than WAT. The DWT, MWT, and CT computation time is faster than that of CCWT, but the denoising performance of DWT, MWT, and CT is lower than that of CCWT. The CCWT used in this study can provide a good balance between computational complexity and denoising performance.

The used method may have an edge over DWT, MWT, and CT in terms of its efficacy in accurately detecting and classifying certain features or patterns in an image. Furthermore, it may be better suited for applications where computation time is not as crucial, such as in medical or scientific research. Therefore, while computation time is a crucial aspect to consider, it is not the sole determinant of a method's applicability. A comprehensive evaluation of the method's performance, accuracy, and suitability for a specific application is necessary before drawing any conclusions.

5 Conclusion

In this study, CCWT, a new wavelet transform method, is used for denoising in color images. CCWT consists of a family of two-dimensional complex wavelets with a phase difference of 2π/3 obtained from the angle relationship between the color axes of the RGB color ring. Since CCWT has better and more useful directional selectivity, it can be used effectively in denoising applications. The efficiency of the method was tested using six different color images named "Lena", "Peppers", "Baboon", "Parrots", "Twins" and "Airplane". Visual qualities were examined to evaluate the results and PSNR, SSIM and MSE values were calculated. The obtained results were compared with DWT, MWT, CT and WAT methods. Additionally, the changes between the calculation times were examined. The experimental results show that CCWT coefficients can effectively eliminate noise due to their rich and practical directional selectivity. For multi-channel color images, it provides better results by denoising at a high rate. Therefore, this method is robust to color images that contain both simple and complex edge information and is suitable for preserving detailed information. In this study, the computation time of the used method and other available approaches are presented, where the used algorithm can achieve a better balance between denoising performance and computational cost. Moreover, the used method may be particularly well-suited for certain applications, including medical or scientific research, where computation time is not of paramount importance.

6 Author contribution statements

In the scope of this study, Mücahit CİHAN contributed by forming the idea, developing the software, the design, reviewing the literature, evaluating the results and writing the manuscript; Murat CEYLAN contributed by forming the idea, evaluating the obtained results, checking the spelling and the content of the article and supervising the study.

Table 1. Evaluation of denoised images with performance metrics as a result of different color test image denoising methods. The best results are shown in bold.

Color Image	σ	DWT			MWT			CT			WAT			CCWT		
		PSNR	*SSIM*	*MSE*	*PSNR*	*SSIM*	*MSE*	*PSNR*	*SSIM*	*MSE*	*PSNR*	*SSIM*	*MSE*	*PSNR*	*SSIM*	*MSE*
Lena	20	27.93	0.95	105.42	29.26	0.97	77.76	29.86	0.97	67.69	29.86	0.97	67.75	**30.18**	**0.98**	**62.96**
	25	26.54	0.94	145.26	27.19	0.95	125.11	29.47	0.97	74.03	29.17	0.97	79.41	**29.63**	**0.97**	**71.59**
	30	25.30	0.92	193.63	25.40	0.93	189.06	27.51	0.95	116.32	27.34	0.95	120.88	**28.01**	**0.96**	**103.77**
	35	24.24	0.91	246.97	23.89	0.90	267.57	24.99	0.92	207.99	24.87	0.91	213.39	**25.75**	**0.93**	**175.35**
	40	23.29	0.88	307.09	22.63	0.87	357.48	22.60	0.87	359.88	22.55	0.86	364.70	**23.44**	**0.89**	**296.65**
Peppers	20	28.74	0.90	27.69	31.15	0.95	50.36	32.13	0.97	40.14	31.74	0.97	43.95	**32.22**	**0.97**	**39.34**
	25	27.12	0.86	127.52	28.51	0.90	92.62	31.13	0.96	50.78	30.67	0.95	56.35	**31.21**	**0.96**	**49.89**
	30	25.79	0.82	173.25	26.31	0.84	153.73	28.76	0.91	87.72	28.51	0.90	93.07	**29.24**	**0.92**	**78.75**
	35	24.64	0.78	226.63	24.68	0.79	224.53	26.07	0.84	163.53	25.90	0.83	169.81	**26.76**	**0.86**	**139.58**
	40	23.67	0.74	283.96	23.32	0.73	308.32	23.63	0.75	287.12	23.45	0.73	298.95	**24.38**	**0.78**	**241.99**
Baboon	20	23.82	0.82	271.73	24.10	0.85	254.87	23.59	0.81	286.92	24.31	0.83	243.04	**24.37**	**0.83**	**239.64**
	25	23.06	0.79	324.19	23.18	0.82	315.29	23.28	0.81	308.04	24.10	0.82	254.95	**24.18**	**0.83**	**250.31**
	30	22.35	0.76	381.43	22.29	0.78	387.20	22.61	0.79	359.67	23.49	0.81	293.64	**23.58**	**0.81**	**287.32**
	35	21.68	0.73	445.64	21.43	0.75	471.09	21.57	0.75	456.79	22.39	0.77	377.77	**22.51**	**0.78**	**367.96**
	40	21.07	0.70	512.23	20.65	0.72	564.03	20.29	0.70	612.91	21.03	0.72	517.38	**21.17**	**0.73**	**500.63**
Parrots	20	28.75	0.83	87.48	30.63	0.90	56.75	32.36	0.94	38.97	31.99	0.94	41.44	**32.38**	**0.95**	**37.92**
	25	27.14	0.78	126.67	27.93	0.82	105.60	31.21	0.91	49.58	30.87	0.91	53.68	**31.39**	**0.92**	**47.65**
	30	25.78	0.74	173.16	25.81	0.75	171.83	28.43	0.83	94.14	28.24	0.83	98.32	**29.08**	**0.85**	**80.94**
	35	24.66	0.69	224.08	24.13	0.69	253.45	25.34	0.73	191.45	25.17	0.71	199.34	**26.22**	**0.76**	**156.51**
	40	23.66	0.66	282.24	22.81	0.64	342.96	22.68	0.63	353.58	22.55	0.61	364.27	**23.53**	**0.66**	**290.46**
Twins	20	29.08	0.80	80.98	31.82	0.88	43.16	33.04	0.91	32.42	32.98	0.91	33.03	**33.05**	**0.92**	**32.48**
	25	27.46	0.76	117.82	28.94	0.82	83.70	31.68	0.88	44.59	31.72	0.88	44.19	**31.95**	**0.89**	**41.92**
	30	26.08	0.72	161.64	26.61	0.75	143.20	29.08	0.82	81.15	29.15	0.83	79.95	**29.70**	**0.85**	**70.37**
	35	24.89	0.69	212.58	24.88	0.70	212.96	26.21	0.75	156.98	26.21	0.74	156.95	**27.02**	**0.77**	**130.26**
	40	23.84	0.65	270.98	23.46	0.65	295.55	23.67	0.66	281.79	23.64	0.66	283.80	**24.47**	**0.69**	**234.32**
Airplane	20	27.78	0.51	109.20	28.61	0.61	90.23	29.63	0.68	71.35	29.45	0.67	74.32	**30.08**	**0.71**	**64.41**
	25	26.43	0.46	149.03	26.68	0.50	140.87	28.84	0.61	85.52	29.08	0.63	81.15	**29.50**	**0.65**	**73.50**
	30	25.29	0.42	194.35	25.02	0.43	206.50	27.25	0.51	123.58	28.04	0.53	102.96	**28.05**	**0.54**	**102.94**
	35	24.31	0.38	243.88	23.66	0.39	283.19	25.17	0.43	200.15	25.18	0.41	199.92	**26.06**	**0.44**	**163.23**
	40	23.48	0.35	296.54	22.57	0.35	364.92	23.11	0.36	322.86	23.01	0.35	330.39	**23.91**	**0.37**	**268.76**

Table 2. Computation time (in seconds) for different color test images using various denoising algorithms.

Method	DWT	MWT	CT	WAT	CCWT
Lena	0.2563	1.0338	1.3635	16.1631	3.5814
Peppers	0.2534	0.9800	1.2865	16.9708	3.6521
Baboon	0.2187	1.0493	1.2824	17.2712	3.6855
Parrots	0.2254	1.0541	1.2012	15.4785	3.9938
Twins	0.2218	1.0263	1.1968	17.4307	3.8949
Airplane	0.2247	1.0567	1.2109	17.4071	3.7199

7 Ethics committee approval and conflict of interest statement

"There is no need to obtain permission from the ethics committee for the article prepared".

"There is no conflict of interest with any person / institution in the article prepared".

8 References

[1] Donoho DL. "De-noising by soft-thresholding". *IEEE Transactions on Information Theory*, 41(3), 613-627, 1995.

[2] Fan L, Zhang F, Fan H, Zhang C. "Brief review of image denoising techniques". *Visual Computing for Industry, Biomedicine, and Art*, 2(1), 1-12, 2019.

[3] Zhang J, Cao L, Wang T, Fu W, Shen W. "NHNet: A non-local hierarchical network for image denoising". *IET Image Processing*, 16(9), 2446-2456, 2022.

[4] Xu J, Zhang L, Zhang D, Feng X. "Multi-channel Weighted nuclear norm minimization for real color image denoising". *In Proceedings of the IEEE International Conference on Computer Vision*, Venice, Italy, 22-29 October 2017.

[5] Singh A, Sethi G, Kalra GS. "Spatially adaptive image denoising via enhanced noise detection method for grayscale and color images". *IEEE Access*, 8, 112985-113002, 2020.

[6] Qin N, Gong Z. "Color image denoising by means of three-dimensional discrete fuzzy numbers". *The Visual Computer*, 39(5), 2051-2063, 2023.

[7] Srisailam C, Sharma P, Suhane S. "Color image denoising using wavelet soft thresholding". *International Journal of Emerging Technology and Advanced Engineering*, 4(7), 474-478, 2014.

[8] Gai S. "Multiresolution monogenic wavelet transform combined with bivariate shrinkage functions for color image denoising". *Circuits, Systems, and Signal Processing*, 37(3), 1162-1176, 2018.

[9] Gai S, Bao Z, Zhang K. "Vector extension of quaternion wavelet transform and its application to colour image denoising". *IET Signal Processing*, 13(2), 133-140, 2019.

[10] Sifuzzaman M, Islam MR, Ali MZ. "Application of wavelet transform and its advantages compared to Fourier transform". *Journal of Physical Science*, 13, 121-134, 2009.

[11] Srisailam C, Sharma P, Suhane S. "Color image denoising using wavelet soft thresholding". *International Journal of Emerging Technology and Advanced Engineering*, 4(7), 474-478, 2014.

[12] Lim BR, Lee HS, Park RH, Yang S. "A wavelet packet-based noise reduction algorithm of NTSC images using CVBS characteristics". *IEEE Transactions on Consumer Electronics*, 55(4), 2407-2415, 2009.

[13] Liu W, Yan Q, Zhao Y. "Densely self-guided wavelet network for image denoising". *IEEE/CVF 2020 Conference on Computer Vision and Pattern Recognition Workshops*, Seattle, Washington, USA, 14-19 June 2020.

[14] Wang Y, Zhang W, Li W, Yu X, Yu N. "Non-additive cost functions for color image steganography based on inter-channel correlations and differences". *IEEE Transactions on Information Forensics and Security*, 15, 2081-2095, 2019.

[15] Chen Y, Li D, Zhang JQ. "Complementary color wavelet: A novel tool for the color image/video analysis and processing". *IEEE Transactions on Circuits and Systems for Video Technology*, 29(1), 12-27, 2017.
[16] Stokley SR. *Historic Look on Color Theory*. Honors Theses, Providence Campus, Johnson & Wales University, Rhode Island, USA, 2018.
[17] Pridmore RW. "Complementary colors theory of color vision: Physiology, color mixture, color constancy and color perception". *Color Research & Application*, 36(6), 394-412, 2011.
[18] Pridmore RW. "Complementary colors: a literature review". *Color Research & Application*, 46(2), 482-488, 2021.
[19] Cihan M, Ceylan M. "Fusion of CT and MR liver ımages using multiresolution analysis methods". *Avrupa Bilim ve Teknoloji Dergisi*, (30), 56-61, 2021.
[20] Unser M, Sage D, Van De Ville D. "Multiresolution monogenic signal analysis using the Riesz–Laplace wavelet transform". *IEEE Transactions on Image Processing*, 18(11), 2402-2418, 2009.
[21] Gai S. "Multiresolution monogenic wavelet transform combined with bivariate shrinkage functions for color image denoising". *Circuits, Systems, and Signal Processing*, 37, 1162-1176, 2018.
[22] Kadri O, Baarir ZE, Schaefer G, Korovin I. "Colour ımage denoising using curvelets and scale dependent shrinkage". *In 2020 IEEE International Conference on Systems, Man, and Cybernetics (SMC)*, Toronto, Canada, 11-14 October 2020.
[23] Mbarki Z, Seddik H. *Rapid Medical İmages Restoration Combining Parametric Wiener Filtering and Wave Atom Transform Based on Local Adaptive Shrinkage*. Editors: Hanen I, Thierry V. Smart Systems for E-Health, 49-77, WBAN Technologies, Security and Applications, 2021.
[24] Giri KJ, Quadri SMK, Bashir R, Bhat JI. "DWT based color image watermarking: a review". *Multimedia Tools and Applications*, 79, 32881-32895, 2020.
[25] Longkumer M, Gupta H. "Image denoising using wavelet transform, median filter and soft thresholding". *International Research Journal of Engineering and Technology*, 5(7), 729-732, 2018.
[26] Unser M, Sage D, Van De Ville D. "Multiresolution monogenic signal analysis using the Riesz–Laplace wavelet transform". *IEEE Transactions on Image Processing*, 18(11), 2402-2418, 2009.
[27] Van De Ville D, Blu T, Unser M. "Isotropic polyharmonic B-splines: Scaling functions and wavelets". *IEEE Transactions on Image Processing*, 14(11), 1798-1813, 2005.
[28] Donoho DL, Duncan MR. "Digital curvelet transform: strategy, implementation, and experiments". *In Wavelet Applications VII*, 4056, 12-30, 2000.
[29] Shensa MJ. "The discrete wavelet transform: wedding the a trous and Mallat algorithms". *IEEE Transactions on Signal Processing*, 40(10), 2464-2482, 1992.
[30] Fiddy MA. "The Radon transform and some of its applications". *Optica Acta: International Journal of Optics*, 32(1), 3-4, 1985.
[31] Aili W, Ye Z, Shaoliang M, Mingji Y. "Image denoising method based on curvelet transform". *In 2008 3rd IEEE Conference on Industrial Electronics and Applications*, Singapore, 03-05 June 2008.
[32] Demanet L, Ying L. "Wave atoms and sparsity of oscillatory patterns". *Applied and Computational Harmonic Analysis*, 23(3), 368-387, 2007.